1-2014

Experimental and Numerical Study of Carbon Fiber Oxidation

Francesco Panerai
University of Kentucky, francesco.panerai@uky.edu

Nagi N. Mansour
NASA Ames Research Center

Jean Lachaud
University of California - Santa Cruz

Alexandre Martin
University of Kentucky, alexandre.martin@uky.edu

Experimental and Numerical Study of Carbon Fiber Oxidation

Digital Object Identifier (DOI)
http://dx.doi.org/10.2514/6.2014-1208

Notes/Citation Information
Published in the *Proceedings of the 52nd AIAA Aerospace Sciences Meeting*, Paper 2014-1208, p. 1-15.

AIAA SciTech
13-17 January 2014, National Harbor, Maryland
52nd Aerospace Sciences Meeting

Experimental and Numerical Study of Carbon Fiber Oxidation

Francesco Panerai*
University of Kentucky, Lexington, KY, USA 40506-0503

Nagi N. Mansour†
NASA Ames Research Center, Moffett Field, CA, USA 94035

Jean Lachaud‡
University of California Santa Cruz, Moffett Field, CA, USA 94035

and Alexandre Martin§
University of Kentucky, Lexington, KY, USA 40506-0503

The oxidation at high Knudsen number of FiberForm®, the matrix material of NASA's Phenolic Impregnated Carbon Ablator, is investigated both experimentally and numerically. The experimental setup consists of a quartz tube through a clamshell heater. Mass loss and recession of carbon preform samples are measured at temperatures between 700 and 1300 K and pressures around 2000 Pa. A volume average fiber-scale oxidation model is used to model the setup and extract the effective reactivity of the material. New values for carbon fiber reactivity are suggested and discussed.

Nomenclature

Symbols

C_p	heat capacity, J/K	$\dot{q}''$	internal heat flux, W/m^2
D	diffusion coefficient, m^2/s	r	fiber radius, m
E	energy, J/kg	R	tube radius, m
E_a	activation energy, J/mol	R	specific gas constant, 8.314 J/(mol·K)
h	enthalpy, J/kg	Re	Reynolds Number
J'	diffusion flux, mol/(m^2·s)	$\dot{\mathbf{r}}$	recession velocity, m/s
J	diffusion flux, kg/(m^2·s)	S	surface area, m^2
k	reactivity, m/s	S_f	specific surface area, m^2/m^3
K	permeability, m^2	T	temperature, K
l	length, m	v	axial velocity, m/s
Le	Lewis number	V	volume, m^3
$\dot{m}'''$	volumetric mass source term, kg/(m^3·s)	z, t	spatial (m) and time (s) coordinates
$\dot{m}$	mass flux, kg/s	Y_i	species mass fraction
M	species molar mass, kg/mol	α, β	stoichiometric coefficients
N	number of fibers	ε	emissivity
p	pressure, Pa	ϵ	volume fraction

*Postdoctoral Scholar, Department of Mechanical Engineering, 261 Ralph G. Anderson Building. Visiting Scientist, Thermal Protection Materials Branch, Mail Stop 234-1, NASA Ames Research Center, Moffett Field, CA, 94035, AIAA Senior Member.
†Chief Division Scientist, Advanced Supercomputing Division, Mail Stop 258-5, AIAA Associate Fellow.
‡Scientist, Silicon Valley Initiatives, NASA Ames Research Park, Building 19, AIAA Senior Member.
§Assistant Professor, Department of Mechanical Engineering - Associate Faculty, Center for Computational Science, 261 Ralph G. Anderson Building, AIAA Senior Member.

η	tortuosity	ρ	density, kg/m^3
κ	conductivity, W/(m·K)	ϕ	porosity
μ	dynamic viscosity, mP	χ	concentration, mol/m^3
Ω	solid molar mass of carbon, kg/mol		
ω	species production rate, kg/(m^2·s)		

Subscripts

0	initial	g	gas
C	carbon	kin	kinetic
cv	control volume	v	virgin
cs	control surface	w	wall
f	fiber		

I. Introduction

For planetary entry missions, charring ablative materials have always been the primary choice for the design of the outer layer of thermal protection systems (TPS). Recent missions have used low density carbon/phenolic composites with success. Low density carbon/phenolic ablators are made of a carbon preform, typically composed of microfibers, impregnated with a pyrolyzing resin matrix based on a phenolic polymer.

This class of materials is capable of dissipating, by thermal and chemical decomposition, the convective heat transmitted to the surface. The gas emitted from the inner decomposition of the matrix is blown into the free stream, creating a partial blockage of the incoming heat-flux. This creates a counter-flow that tends to decrease the net mass transfer of reacting gases to the surface, thickening the boundary layer and pushing the bow shock away from the wall. The chemical composition at the surface of the vehicle is significantly changed in the process.[1]

The composition of the gases in the boundary layer also greatly influences surface reactions. For charring ablators, it has been suggested that reactions do not occur at the surface of the material but within a thin layer near the surface.[2] The impregnating phenolic phase in this region pyrolyzes and oxidizes very quickly, leaving the carbon fibers exposed to the surrounding gas. Because of the high porosity of the material, reacting gas from the outer flow, oxygen in the case of Earth entries, diffuses into this layer and reacts with the carbon fibers, removing matter from them until they completely vanish. High-fidelity ablation models are being developed to account for these phenomena for the purpose of sizing TPS material thickness.[1,2,3]

In this context, there is a need to update and modernize past experiments, such as those presented in Ref. 4, and propose new, validated pyrolyzing chemistry and surface reaction models specific to the new class of low-density carbon/phenolic composites. With this goal in mind, the objective of this work is to measure the reactivity of carbon fibers and use numerical simulation to extract its value with improved accuracy. Experiments are performed in the flow-tube reactor facility at NASA Ames Research Center, on the matrix of PICA, the Phenolic Impregnated Carbon Ablator TPS used by NASA for exploration missions. Temperatures between 700 and 1300 K and a testing pressure of 2000 Pa are considered. First, the setup and the main outcomes of the experimental measurements are described. A material response model used to simulate the flow-tube tests is then presented. New values for carbon fiber reactivity are suggested, and finally a comparison between computations and measurements is discussed.

II. Experiment

II.A. Test Setup

Experiments are performed in the NASA flow-tube reactor sketched in Fig. 1. A photograph of the experimental arrangement is shown in Fig. 2. The setup is similar to that presented in Panerai *et al.*,[5] with refinement to the pressure and temperature measurements. The facility consists of a quartz main tube, connected to a right angle 2.5 cm diameter side arm, where the test section is located. High purity air (Ultra Zero Grade 99.999%, Matheson Tri-Gas®, San Jose, CA, United States) and helium (Ultra High Purity Grade 99.999%, Matheson Tri-Gas®, San Jose, CA, United States) are supplied and regulated using metering valves and calibrated mass flow meters (FM-360, Tylan Corp., Torrance, CA, United States). To operate the facility as a flow-tube the main arm is sealed downstream of the intersection by a Teflon® valve,

kept closed throughout the test. The central part of the quartz side-arm is enclosed in a clamshell electric furnace, spanning a region of approximately 470 mm, and providing temperatures up to 1500 K. The test specimen is placed at the middle section of the furnace prior to testing, using glass holders and extension tubes.

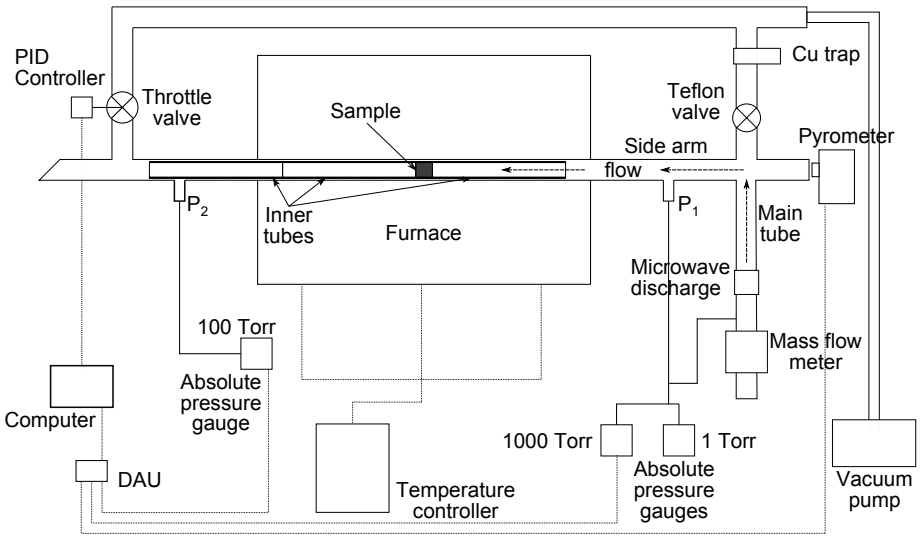

Figure 1. Schematic of the NASA Ames flow-tube test setup.

The system is evacuated using a mechanical pump attached just before the dead-end of the side-arm. The pressure is monitored at the two locations labeled as P1 and P2 in Fig. 1, respectively upstream and downstream of the sample, using capacitance manometer gauges (622B Baratron®, MKS Instruments, Andover, MA, United States), calibrated prior to the experiments. The accuracy of these measurements, considering the fluctuation of the measured signal, is ±100 Pa. Two sensors with an operational range of 1 and 1000 torr measure the pressure p_1 at port P1 and provide a feedback to a PID system. This controls the throttle valve at the side-arm outlet and is used to adjust p to the desired value. A sensor with a 100 torr range measures the pressure p_2 at port P2. An infrared pyrometer (M90H, Mikron Infrared, Oakland, NJ, United States) is placed at the upstream extremity of the side-arm and focused on the flow-facing surface of the sample. The pyrometer is used to measure the surface temperature of the material and to quantify the amount of overheating caused by the onset of exothermic carbon oxidation reactions, when the flow is switched from helium to air and the oxidation phase starts. The pyrometer instrument operates from 873 K to 3273 K and detects the normal radiance emitted from the surface between 0.78 and 1.06 μm. From the radiance, the temperature can be deduced if the emissivity of the sample's surface and the transmissivity of the Brewster end-window between the instrument and the target are known. For the present experiment we chose to perform an in-situ calibration in helium flow, to prevent chemical reactions with the material while the sample's temperature equilibrates to the set temperature of the furnace. The calibration is by executed running a constant helium flow at ≈ 0.3 mg/s, increasing the temperature in steps of ≈ 50 K between 900 and 1300 K, and recording the voltage output of the pyrometer versus the furnace temperature. The validity of this calibration is supported by no variations measured in the mass of the sample before and after high temperature exposure and by scanning electron microscopy (SEM) measurement showing an unchanged fiber structure before and after testing. Both confirm that no reactions, hence no temperature variations, have occurred during the run. Pyrometer measurements are believed to be accurate to ±1%. Both the pressure sensors and the pyrometer are interfaced to the computer system by means of an analog data acquisition card (NI USB-6009, National Instruments, Austin, TX, United States) that allows continuous recoding of temperature and pressure during the test. The acquisition frequency used is at 2 Hz.

The material, FiberForm®, is an industrial carbon preform manufactured by Fiber Materials Inc. (Biddeford, ME, United States) for industrial thermal furnace insulation. The sample geometry is a 22 mm diameter, 25.4 mm height cylinder (plug). The specimen is interference-fit into a glass holder placed at the middle section of the heating furnace. One 220 mm long glass tube is placed upstream of the sample holder, and a second tube downstream of the sample holder, both contacting the holder to avoid facing steps and to

ensure a fully developed flow. In contrast to the work presented in Ref. 5, where carbon tube models (hollow cylinders) were tested, the usage of a plug test article ensures that all of the flow is through the material.

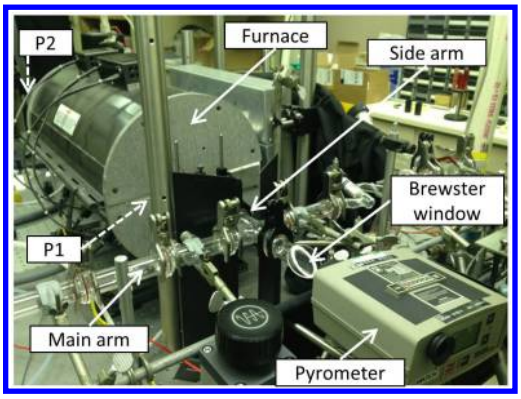

Figure 2. Photograph of of the flow-tube setup.

The test procedure consists of sealing the tubes, evacuating the system to a base pressure below 10 Pa, and feeding it with a low helium flow (below 0.03 mg s^{-1}) while the furnace is heating up to the target temperature condition. The supply of He ensures that no oxidation reactions occur during the transient heating phase. Once the temperature is stabilized, the He flow is interrupted, the chamber is evacuated down to 100 Pa, and dry air is started at the desired rate. The test gas supply causes the pressure to rise to the target value, when the regulation is taken over by the PID controller that adjusts the suction rate of the mechanical pump downstream the samples. Mass flow and pressure are maintained constant throughout the test time. The experiment ends with a final evacuation of the test section to below 100 Pa and a cooling phase during which He is again flowed in to stop the oxidation reactions.

Table 1. Summary of flow tube test conditions: pressure at port P1 (upstream), temperature, oxidation time, mass flow rate, velocity, gas density, gas viscosity and Reynolds number

Sample #	p_1, Pa	T, K	t, min	$\dot{m}$, mg/s	v, m/s	ρ_g, kg/m^3	μ_g, mP	Re
a1	1880	700	60	2.21	0.583	0.00995	0.34288	3.72
a2	1933	800	60	2.21	0.666	0.00871	0.37563	3.40
a3	1920	900	60	2.21	0.750	0.00774	0.40688	3.14
a4	1960	1000	60	2.21	0.833	0.00697	0.43688	2.92
a5	1987	1100	60	2.21	0.916	0.00633	0.46572	2.74
a6	1973	1200	60	2.21	0.999	0.00581	0.49355	2.59
a7	1900	1300	60	2.21	1.083	0.00536	0.52059	2.45

The test conditions are detailed in Table 1. Experiments are performed at temperatures from 700 to 1300 K and a static pressure of $\approx$ 2000 Pa, for a total oxidation time of 1 h. Flow conditions are calculated using the Chemical Equilibrium with Applications (CEA) code[6] from NASA Glenn Research Center. Reynolds number $\mathrm{Re} = \rho u D/\mu$, based on the 22 mm tube diameter, is below 4 at all test conditions, indicating a fully laminar pipe flow.

Mass measurements of the samples are performed using an analytical balance (AB104S, Mettler-Toledo, LLC, Columbus, OH, United States) with $\pm$0.1 mg accuracy. A caliper is be used to document changes in length Δl (recession), with $\pm$0.1 mm precision. The bulk density of the material is estimated as the ratio between the mass measured with the balance and the volume calculated from caliper measurements, assuming the samples to be perfect cylinders. Initial densities of the virgin specimens are calculated to be around 165 kg m^{-3}, with an uncertainty of $\pm$6 kg m^{-3}. An environmental scanning electron microscope (XL30 ESEM, FEI, Hillsboro, OR, United States) is used to characterize the morphology of the fiber before and after the oxidation tests.

II.B. Experimental Results

The exposure of the material to high temperature and to an oxygen-rich flow transforms solid carbon into gaseous carbonaceous products, and mass is lost. Figure 3 shows the photograph of a sample (a6) before and after oxidation (at 1200 K). Impurities deposited at the surface are observed on the tested materials. Previous investigations suggested that these are calcium carbonate residues.[5,7]

Micrographs of the FiberForm® are shown in Fig. 4. The virgin material is composed of fibers with diameters between 9 and 13 µm and lengths between 100 and 500 µm. Bundles or clusters, where multiple fibers are bonded, are observed at several locations. SEM images of the oxidized material shows fiber pitting typical at the flow-tube Knudsen regime. Mass is lost at localized sites where oxygen molecules react with carbon.

In Fig. 5 the surface temperature measured with the pyrometer is plotted as a function of time for sample a7, tested at a furnace temperature of 1300 K. During the heating phase, with He flow, the temperature of the sample gradually increases to the target value. Enough time is given for the temperature to stabilize to the set value. As the gas flow is switched from He to air and the oxidation phase is started, a jump in surface temperature is observed (a magnified view is shown on the right plot of Fig. 5). As predicted, the jump is due to the exothermic nature of oxidation reactions, causing the surface temperature to increase. This is also confirmed by the numerical predictions presented later in the paper. Values of $\Delta T = T_w - T$, where T_w is the temperature of the surface and T the target furnace temperature, are found to be between 9 and 13 K.

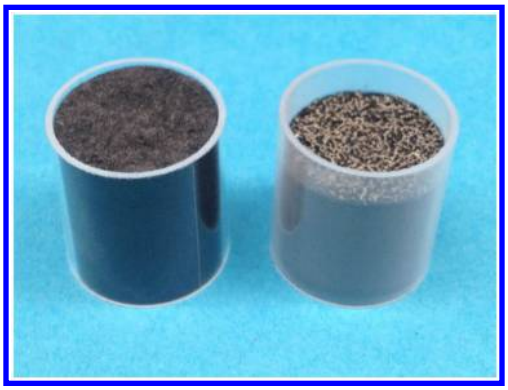

Figure 3. Photograph of virgin (left) and oxidized (right) FiberForm® samples.

Percent mass loss and recession are plotted in Fig. 6. As expected, mass loss is higher at higher temperature. Similarly to what was found in previous experiments,[5] the mass loss rate seems to slow at temperatures between 900 and 1100 K, and then increases again at higher temperatures. This behavior shall be further investigated in the future with dedicated tests.

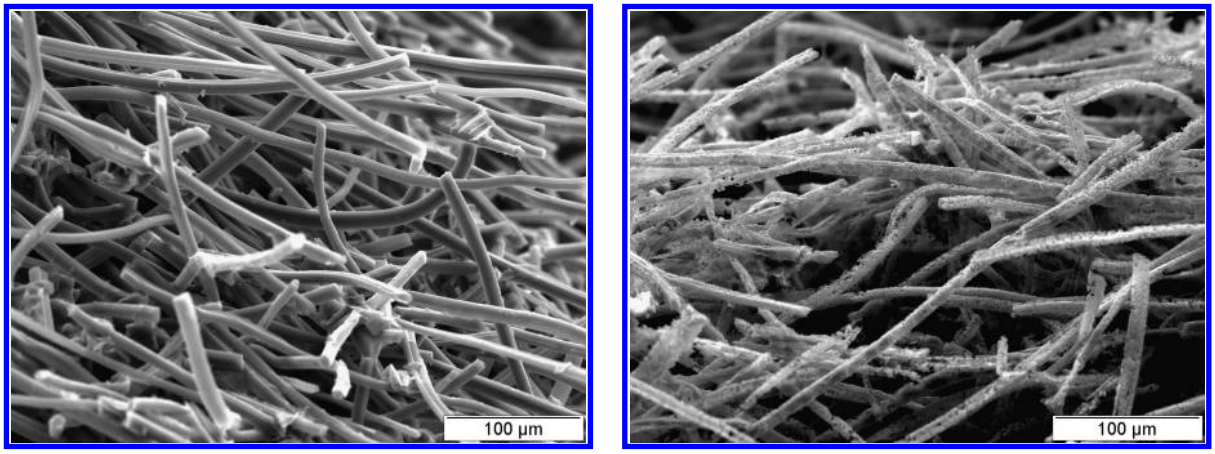

Figure 4. Scanning electron micrographs of virgin (left) and oxidized (right) FiberForm®.

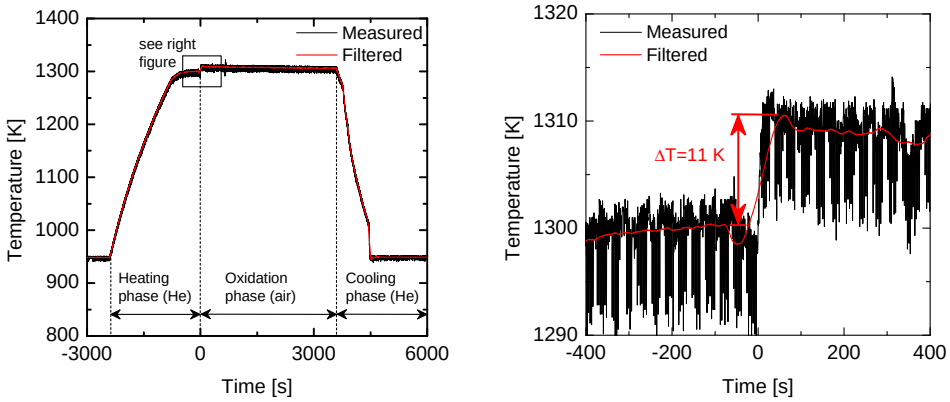

Figure 5. Example of pyrometer surface temperature measurement for sample a7 (1300 K). Global behavior (left) and closer view of temperature jump due to exothermic oxidation reactions (right).

No overall surface recession of the sample is observed for temperatures $\leq$900 K. At these conditions, oxidation is purely a volumetric process. The time scale of reactions is longer than that of diffusional transport in the porous medium (reaction-limited regime, small Thiele numbers).[5] Higher temperatures result in faster reactions and the in-depth oxidation processes slow until oxidation becomes a purely surface phenomenon,

where all of the available oxygen is consumed at the surface (diffusion-limited regime, high Thiele). For the present experiments, even at temperatures above 900 K, a small surface recession is observed (less than ≈20% of the total length is lost at the maximum temperature of 1300 K), suggesting that reaction-limited oxidation prevails at all test conditions. This is also consistent with previous experiments on FiberForm® where, for similar test conditions, Thiele numbers below 10^{-1} were calculated.[5]

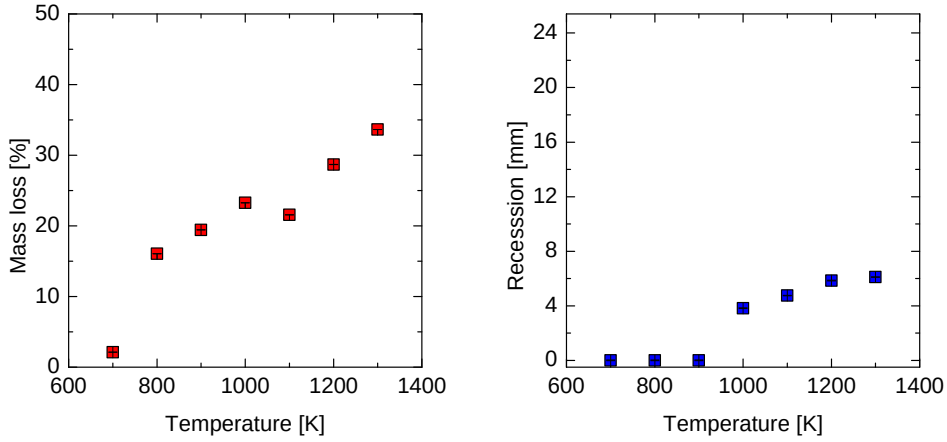

Figure 6. Percent mass loss Δ_m/m_0 (left) and surface recession Δl (right) as a function of temperature.

Measurements of the pressure at ports P1 and P2 allow determination of the pressure drop across the sample as the material oxidizes. An example is shown in Fig. 7 for test a6 at 1200 K. An initial phase where the pressure fluctuates is noticed, until the PID control achieves the target p1 value. One can clearly observe that, once stabilized, the pressure p1 is maintained constant throughout the experiment, while the pressure p2 slightly increases as the test progresses. As expected, the increase in p2 is faster at higher temperatures. This is shown in Fig. 8, where the evolution of the pressure drop Δp is plotted versus time, at 1200 K (the same test shown in Fig. 7), as well as at 700 K (test a1) where no recession and very small mass loss are measured. At 700 K, p2 remains constant during the test and no variation in Δp is measured.

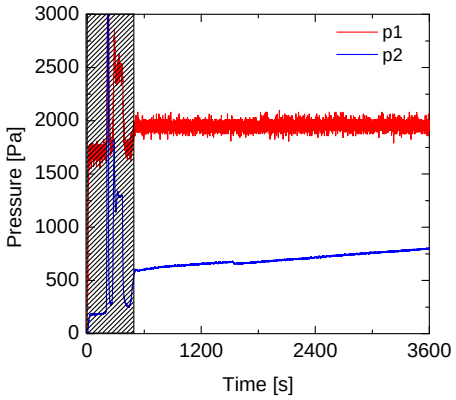

Figure 7. Time evolution of pressure measured at P1 (upstream the sample) and P2 (downstream) sections, for test a6 at 1200 K.

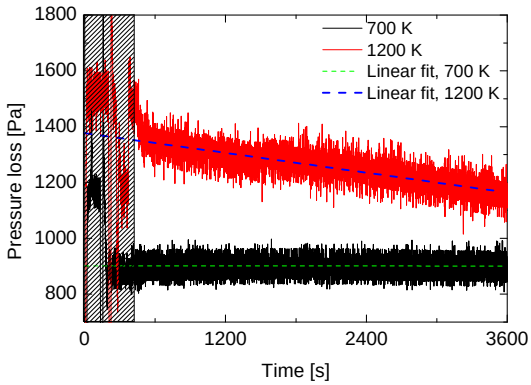

Figure 8. Time evolution of pressure difference $\Delta p = p_1 - p_2$ across the sample, for test a6 at 1200 K (oxidized) and test a1 at 700 K (non oxidized).

A linear regression is used to fit the data and to determine the Δp at $t = 0$ s. From this value the initial permeability K of the FiberForm®, used later for the simulations, is determined by integration of Darcy's law, using the Klinkenberg model.[8] The integration of Darcy's law holds under the assumption that the material properties are constant in the direction of the integration, which for the present experiment is only valid at $t = 0$ s. Future investigations shall be aimed at the characterization of in-depth changes in microstructure and density as the material oxidizes. Micro-tomography appears to be a suitable tool for such characterization.[9]

III. Numerical Modeling

III.A. Material Response Model

III.A.1. Chemical equilibrium material response

The material response code used in the present study has been developed and validated over the last few years[10] and was recently adapted to account for finite-rate chemistry.[11] The code models gas flow through porous media by solving the conservation equations written in moving coordinates:

Mixture Energy Equation

$$\frac{d}{dt}\int_{cv}\rho E dV - \int_{cs}\rho h\vec{v}_{cs}\cdot\vec{n}dS + \int_{cs}\phi\rho_g h_g\vec{v}_g\cdot\vec{n}dS + \int_{cs}\vec{q}''\cdot\vec{n}dS + \int_{cs}\phi\sum_k \vec{J}_k h_{g_k}\cdot\vec{n}dS - \int_{cv}\phi\vec{v}_g\cdot\nabla p\, dV = 0 \quad (1)$$

Solid Phase Equation

$$\frac{d}{dt}\int_{cv}\rho_s dV - \int_{cs}\rho_s\vec{v}_{cs}\cdot\vec{n}dS - \int_{cv}\dot{m}_s'''dV = 0 \quad (2)$$

Gas Phase Continuity Equation

$$\frac{d}{dt}\int_{cv}\phi\rho_{gk}dV - \int_{cs}\phi\rho_{gk}\vec{v}_{cs}\cdot\vec{n}dS + \int_{cs}\phi\rho_{gk}\vec{v}_g\cdot\vec{n}dS - \int_{cs}\phi\vec{J}_k\cdot\vec{n}dS - \int_{cv}\left(\dot{m}_{gk}''' + \omega_k\right)dV = 0 \quad (3)$$

Momentum Equation: Darcy's Law

$$\frac{\partial P}{\partial z} = -\frac{\mu}{K}\phi v_g \quad (4)$$

The first terms in Eqs. (1) to (3) account, respectively, for energy, solid mass, and gas mass content, and the second term accounts for the grid motion. The third terms in Eqs. (1) and (3) account for the gas flux, and the last terms in Eqs. (2) to (3) for the source term. The fourth term of Eq. (1) accounts for heat conduction, modeled according to Fourier's Law:

$$\dot{q}'' = -\kappa\frac{\partial T}{\partial z}$$

The kinetic energy, $\tilde{E}_{kin} = v_g^2/2$, of the pyrolysis gas, which is usually negligible in most material response code applications, becomes quite important in this simulation. Usually, the gas phase contribution to the energy equation is a few orders of magnitude less than the terms related to conduction through the solid material, mostly because of the great difference in density and heat capacity. However, in the present application the solid is almost at a constant temperature, and the oxidation gas is modeled before and after it enters the constant temperature porous sample, in which case, the kinetic energy contribution is of the same order of magnitude as the other terms. The kinetic energy is therefore calculated using:

$$\frac{d}{dt}\int_{cv}\phi\rho\tilde{E}_{kin}dV + \int_{cs}\phi\rho_g\tilde{E}_{kin}\vec{v}_g\cdot\vec{n}dS - \int_{cs}\phi\rho\tilde{E}_{kin}\vec{v}_{cs}\cdot\vec{n}dS + \int_{cv}\phi\vec{v}_g\cdot\nabla p\, dV = 0$$

In theory, Darcy's law is only valid for porous flow. However, it is possible to adapt it for non-porous media by adjusting the value of the permeability. Since the average velocity of a steady, laminar, fully developed flow in a pipe of radius R is given by

$$\bar{v} = -\frac{\partial P}{\partial z}\frac{R^2}{8\mu},$$

using Eq. (4), it can be seen that for a fully developed laminar flow inside a tube, for which $\phi = 1.0$, since there is no porous material, Darcy's formulation can be used by simply setting the permeability, $K = R^2/8$.

III.A.2. Finite Rate Chemistry

In the gas conservation equation (Eq. (3)), k represents one of the species of the finite rate chemistry model; there is such an equation for all species considered, and $\sum_k \rho_{gk} = \rho_g$. The term $\dot{m}'''_{gk}$ relates to the mass fraction of the solid that is transferred to species k and ω_k relates to the amount of species k that is created using the finite-rate chemistry model. The latter source term is evaluated by:

$$\omega_k = M_k \sum_{j=1}^{m} (\beta_{kj} - \alpha_{kj}) \left[k_{fj} \prod_{i=1}^{q} \left(\frac{\rho_i}{M_i} \right)^{\alpha_{ij}} - k_{rj} \prod_{i=1}^{q} \left(\frac{\rho_i}{M_i} \right)^{\beta_{ij}} \right]$$

where α_{ij} and β_{ij} are, respectively, the stoichiometric coefficients for product and reactants i of reaction j, and M_j is the molar mass of species j. The forward k_f rates are calculated using an Arrhenius equation:

$$k_f = k_0 T^{-s} \exp\left(-E/RT\right) \tag{5}$$

in which the coefficients k_0, s and E are the typical Arrhenius coefficients. The species mass diffusion, J_k, is modeled using Fick's Law:

$$J_k = -\rho \frac{D_k}{\eta} \frac{\partial Y_k}{\partial z}$$

where Y_l is the mass fraction of species k and η is the tortuosity. This equation is implemented in a way that enforces that the sum of all the diffusion fluxes are zero, if the models used to calculate the species diffusion D_k require it.[12] A mass diffusion term is also present in the energy equation.

III.B. Thermodynamical and Transport Properties

The chemical properties of each individual species are evaluated using the thermodynamic curve fits obtained from Ref. 6. This provides a value for the heat capacity C_{Pk} of each species, as well as enthalpy h_k, heat of formation h_k^0, and entropy S_k. These values are also used to calculate the equilibrium values if reversible reactions are used in the finite-rate chemistry model. The single species viscosity μ_k and conductivity κ_k are obtained using curve fits compiled in Ref. 13. Because of the lack of data available for multi-component viscosity, that property of the gas mixture is evaluated using the simple approximation to the first term of the Chapman-Enskog expansion, Wilke's mixing rule:[14]

$$\mu = \sum_k \frac{X_k \mu_k}{\phi_k} \quad \text{and} \quad \kappa = \sum_k \frac{X_k \kappa_k}{\phi_k}$$

where X_k is the molar fraction and ϕ_k is given by:

$$\phi_k = \sum_r X_r \frac{\left[1 + \sqrt{\frac{\mu_k}{\mu_r}} \left(\frac{M_r}{M_k} \right)^{1/4} \right]^2}{\sqrt{8 \left(1 + \frac{M_k}{M_r} \right)}}$$

Because no binary collision data is used in this approach, the diffusion coefficient D_k is obtained using the constant Lewis number approximation:

$$D_k = D = \frac{\text{Le } k}{\rho C_P}$$

III.C. Volume-Averaged Fiber-Scale Oxidation

It has been shown that the so-called surface ablation is more likely to be a volumetric phenomenon during atmospheric entry.[15] Lachaud and Mansour[15] have theorized, and later demonstrated, that the oxygen from the surrounding flow actually penetrates the porous material over a small distance and oxidizes the material from within. The recession rate, therefore, is not based on the macroscopic surface that is exposed to the flow field, but on the surface of the carbon fibers, thus the porosity of the material. In this study, the chemical oxidation is therefore only modeled by using a set of heterogeneous reactions:

$$\mathrm{C_{(s)}} + \mathrm{O_2} \longrightarrow \mathrm{CO_2}$$

$$C_{(s)} + 1/2O_2 \longrightarrow CO$$
$$C_{(s)} + CO_2 \longleftrightarrow 2CO$$

In the range of interest for an ablating charring ablator, all three of these reactions are important. The third reaction, the so-called "Boudouard reaction", dictates the ratio of CO/CO_2 created during the oxidation process (gasification). Below 973 K, the Boudouard equilibrium temperature,[16] mostly CO_2 is produced. Conversely, CO is the dominating product when the temperature is higher than 973 K. If the temperature oscillates around that equilibrium point, an interesting phenomenon may occur. As the gas cools down, the transformation of the CO into CO_2 leads to soot formation. The gases formed by these heterogeneous reactions are also expected to interact in the gas phase. Depending on the temperature, various exchange reactions between N_2, O_2, CO_2 and CO are likely to occur.

For the test conditions of this study, only the second oxidation reaction is considered. No gas phase kinetics are expected to take place. The reaction rate is expressed as the parameter k_f, and the diffusion flux of incoming oxygen is equivalent to the flux of outgoing carbon monoxide:

$$-J'_{\mathrm{CO}} = J'_{\mathrm{O_2}} = k_f \chi_{\mathrm{O_2}}$$

where $\chi_{\mathrm{O_2}}$ is the molar concentration of oxygen. Thus, the surface recession of an individual fiber of radius r is expressed in terms of the molar diffusion of carbon monoxide J_{CO} at the surface:

$$\dot{\mathbf{r}} = \Omega J'_{\mathrm{CO}} \mathbf{n}$$

where $\Omega = M_C/\rho_C$ is the solid molar mass of the carbon and $\mathbf{n}$ is the outward normal vector of the fiber surface. Assuming that the fibers are perfectly cylindrical and that they recess uniformly, this equation can be expressed in 1D as:

$$\frac{dr}{dt} = -\Omega k_f \chi_{\mathrm{O_2}} \tag{6}$$

The volumetric approach used here assumes that the fibers enclosed in a control volume V_T have a representative initial radius and are distributed homogeneously. The control volume can therefore be split into the volume occupied by the fibers V_f and the volume "occupied" by the pores V_p. These can be expressed in terms of volume fraction:

$$\frac{V_f}{V_T} + \frac{V_p}{V_T} = \epsilon + \phi = 1$$

where ϵ is the fiber volume fraction and ϕ the porosity. The volume occupied by N fibers of radius r and length l_f is therefore given by $V_f = N\pi r^2 l_f$. As the fibers oxidize, the fiber volume fraction changes and can be expressed as a function of the initial volume fraction:

$$\epsilon = \epsilon_0 \frac{r^2}{r_0^2}$$

In order to be included in the material response code, these relations have to be expressed in terms of the bulk density of the carbon matrix. This density can be expressed in terms of the mass of all fibers enclosed in the control volume:

$$\rho_s = \frac{m_f}{V_T} = \frac{N\pi r^2 l_f}{V_T}\rho_{\mathrm{C}} = \epsilon \rho_{\mathrm{C}}$$

where ρ_{C} is the density of solid carbon (not to be confused with the bulk density). The bulk density change, due to the oxidation of fibers, is therefore:

$$\frac{\partial \rho_s}{\partial t} = -\frac{\epsilon_0}{r_0^2} 2r\rho_{\mathrm{C}} \frac{\partial r}{\partial t}$$

By using the parameter S_f, which represents the volumetric surface of occupancy by the fibers and is defined as

$$S_f = \frac{N\pi 2Rl_f}{V_T} = 2\frac{\epsilon_0}{r_0^2} r, \tag{7}$$

as well as Eq. (6), this equation becomes:

$$\frac{\partial \rho_s}{\partial t} = -k_f S_f M_{\mathrm{C}} \chi_{\mathrm{O_2}} \tag{8}$$

or, if re-arranged in terms of ρ_s:

$$\frac{\partial \rho_s}{\partial t} = -2k_f \frac{M_C}{M_{O_2}} \frac{\rho_{O_2}}{r_0} \sqrt{\frac{\epsilon_0}{\rho_C}} \sqrt{\rho_s}$$

This expression can be solved analytically to give the evolution of the bulk density over time step Δt:

$$\rho_s^{(t)} = \left(\sqrt{\rho_s}^{(t-1)} - k_f \frac{M_C}{M_{O_2}} \frac{1}{r_0} \sqrt{\frac{\epsilon_0}{\rho_C}} \int_{(t-1)}^{(t)} \rho_{O_2} dt \right)^2 \tag{9}$$

The amount of oxidation in the gas phase cannot be solved analytically and must be integrated as a source term in Eq. (3):

$$\dot{m}'''_{O_2} = -\rho_{O_2} \frac{M_{O_2}}{M_{O_2}} S_f k_f \ , \quad \dot{m}'''_{CO_2} = \rho_{O_2} \frac{M_{CO_2}}{M_{O_2}} S_f k_f \tag{10}$$

It is to be noted that Eq. (8) can be re-written in the same form, to give:

$$\dot{m}'''_C = -\rho_{O_2} \frac{M_C}{M_{O_2}} S_f k_f$$

III.D. Numerical Approach

The code solves Eqs. (3) and (1) implicitly on an arbitrary contracting grid employing Landau coordinates. Equation (2) is straightforward and does not need to be solved numerically. Darcy's law, Eq. (4), is explicitly solved for v_g and directly integrated in the gas-phase continuity equation.

Newton's method for nonlinear systems is used to solve each of the equations, and an iterative process is performed over the whole set until convergence is attained. This method, called block Gauss-Seidel, converges linearly and is quite efficient when applied to a reduced set of equations. In the chemical equilibrium version of the code, only two equations are needed to be solved numerically and therefore this method is appropriate. In the chemical non-equilibrium version, the number of equations is dependent on the number of species and therefore increases the iterative process immensely. Instead of using block Gauss-Seidel on each of the $1+N_S$ equations, where N_S is the total number of species, the method is only applied to the energy and the total gaseous mass conservation equation. However, in this second equation, the mass conservation of each species is solved at once, using the Newton method. This method requires the inversion of a block tri-diagonal system of equations, instead of a simple tri-diagonal.

To account for fiber oxidation, Eq. (9) is solved directly over time step Δt to calculate the solid decomposition and the surface function S_f. The latter quantity is then used as a source term in the gas phase equation (Eq. (3)), by way of Eq. (10).

III.E. Problem Description

The material response code is adapted to model the flow tube reactor experimental arrangement described in Section II. The test conditions for the simulations are taken from Table 1. In Table 2 the material properties are summarized. The inlet mass flow rate is enforced in front of the samples. As in the experiment, the downstream pressure is not fixed, but modulated every 0.01 seconds (or more, if the time steps are greater than 0.01 s) so that the inlet conditions are preserved.

A porosity of 0.85 is imposed for the virgin FiberForm®, as calculated from micro-tomography measurements on the material.[9] The bulk density used for the simulations is that computed from mass and volume measurements of the actual specimens (≈165 kg/m^3). The resulting carbon density for a volume fraction of $\epsilon = 0.15$ is $\rho_C = \rho_{bulk}/\epsilon \approx 1100$ kg/m^3, lower than values used in existing literature.[2] The initial fiber radius is set to 5.5 µm, which is an average value obtained from microscopic analysis of FiberForm®.

The tortuosity is set to 1.15 for the virgin state of the sample and assumed to decrease linearly to 1.00 when the material reaches a porosity of 1.0. The permeability K of virgin FiberForm® at high temperature is computed by integrating Darcy's law across the sample, using the pressure drop measured at time $t = 0$ s.[8] K is then assumed to decrease exponentially to the free stream value as the porosity linearly increases. As mentioned earlier, because the code uses Darcy's law to model the momentum transport, this would translate into a permeability of $\approx 10^{-5}$ m^2. However, such a high value of the permeability considerably raises the numerical stiffness of the code and prevents the solution from being obtained in a timely manner. However, since both the mass flow rate and the pressure are imposed at the inlet and because the gas velocity

is relatively slow (Reynolds number $\lesssim 4$), it can easily be shown that using a smaller permeability, even 2 or 3 orders of magnitude smaller, only affects the pressure in the flow tube by an insignificant amount.[17]

Table 2. Summary of Fiberform® properties used for the numerical simulations: porosity, bulk density, carbon density, fiber radius, tortuosity, permeability, emissivity. The subscript 0 indicates these are properties initial (non oxidized) materials properties.

Sample #	ϕ_0	$\rho_{bulk,0}$, kg/m^3	$\rho_{C,0}$, kg/m^3	r_0, µm	η_0	$K_0 \times 10^{-9}$, m^2	ε
a1	0.85	163.9	1092.92	5.5	1.15	0.7672	0.9
a2	0.85	163.8	1091.69	5.5	1.15	1.0124	0.9
a3	0.85	163.5	1089.99	5.5	1.15	1.3987	0.9
a4	0.85	164.4	1095.77	5.5	1.15	1.3720	0.9
a5	0.85	165.0	1100.32	5.5	1.15	1.0721	0.9
a6	0.85	155.8	1038.67	5.5	1.15	1.3786	0.9
a7	0.85	167.8	1118.59	5.5	1.15	1.5892	0.9

Another key aspect of the simulation is that a section of the tube must be modeled in order for a reasonable diffusion-driven boundary layer to develop in front of the sample. This is necessary as the flow travels at such a small velocity (between 0.5 and 1 m/s, see Table 1) that the diffusion velocity is not negligible. This means that, as the sample oxidizes, a significant amount of product will diffuse in the opposite direction of the flow, therefore reducing the amount of available reactants. It is clear that the accuracy of the diffusion coefficients plays a significant role in the surface recession. It was previously shown[11] that the absence of such a buffer zone causes significant changes in the results, going from surface recession overestimation to flow reversal. For different reasons, it is also imperative to model a section of the tube after the sample. This allows the energy released by the oxidation chemistry to be properly convected away by the flow and so not remain near the test article. The importance of this modeling aspect was also demonstrated in Martin.[11] For these reasons, a tube length of 0.7 meter is used upstream and downstream of the sample.

Finally, a re-radiating source term is applied at both ends of the sample, $q_{re-rad} = F_{s,t}\varepsilon(T_w - T_{inf})^4$, where the emissivity ε is assumed to be 0.9, T_{inf} is set to the furnace temperature, and the view factor $F_{s,t}$ between the surface and the tube walls is calculated according to the distance between the sample's surface and the surrounding surfaces. The re-radiating term mitigates the increases of energy within the sample.

III.F. Numerical Results

Results of the simulation of case a6 at 1200 K are presented in Fig. 9, showing species mass fractions and production rate inside the FiberForm® sample, at four different oxidation times. No significant change is observed. Species production rates and concentrations reach steady state immediately and remain constant during the test, confirming that oxidation at the experimental Knudsen number is mostly a reaction-limited process.

Since the code also solves the energy equation, results for the temperature of the gas are also presented. Because oxidation is an exothermic process, a rise in temperature of ≈ 8.5 K is observed in Fig. 10, similar to the jump measured with the pyrometer during the experiments (7.5 K for test a4). In Fig. 10(b), showing the distribution of temperature inside the sample, a maximum inside the material is found. This is caused by the presence of a negative source term at the surface, dissipating the exothermic oxidation heat accumulated inside via re-radiation. The maximum is of the order of 10 K above the surface temperature. It is acknowledged that the current fiber-scale model does not account for radiative heat exchange between the fibers (i.e., in depth in the material). Modeling re-radiation between fibers should be considered in the future for more accurate predictions of temperature distributions inside the material.

IV. Comparison and Discussion

Numerical simulations and experiments are compared in Table 3. The value of the fiber reactivity k_f is that providing the closest reproduction of the percent mass loss. Since permeability values computed from $p2$ at $t = 0$ s are assumed for the simulation, the simulations yield a good reproduction of the initial downstream pressure. Computed values of the temperature jump at the surface are similar to those measured during the experiments. Discrepancies are found between the recession of the surface, which is predicted

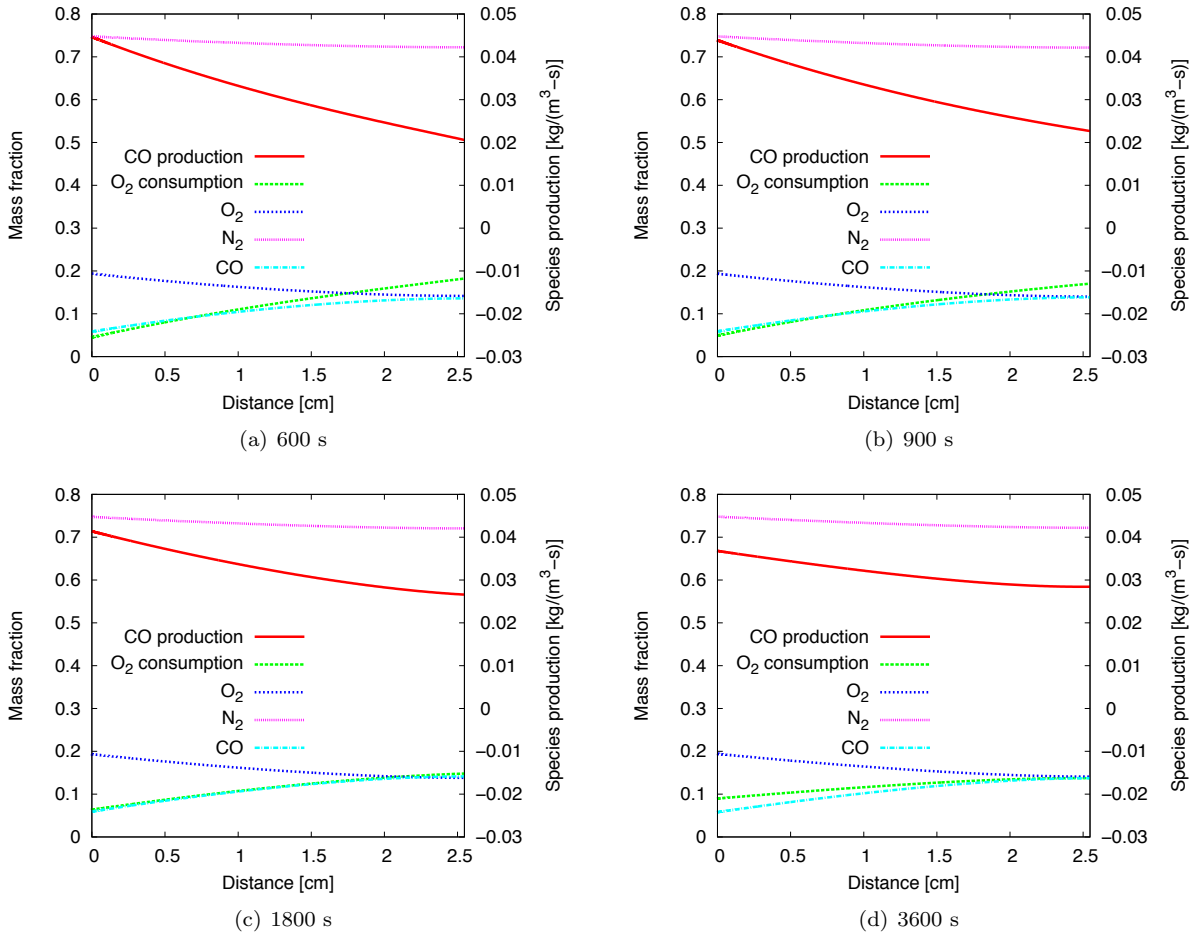

(a) 600 s (b) 900 s

(c) 1800 s (d) 3600 s

Figure 9. Time dependent gas mass fraction and species production rate inside the FiberForm® sample for test a6 at 1200 K.

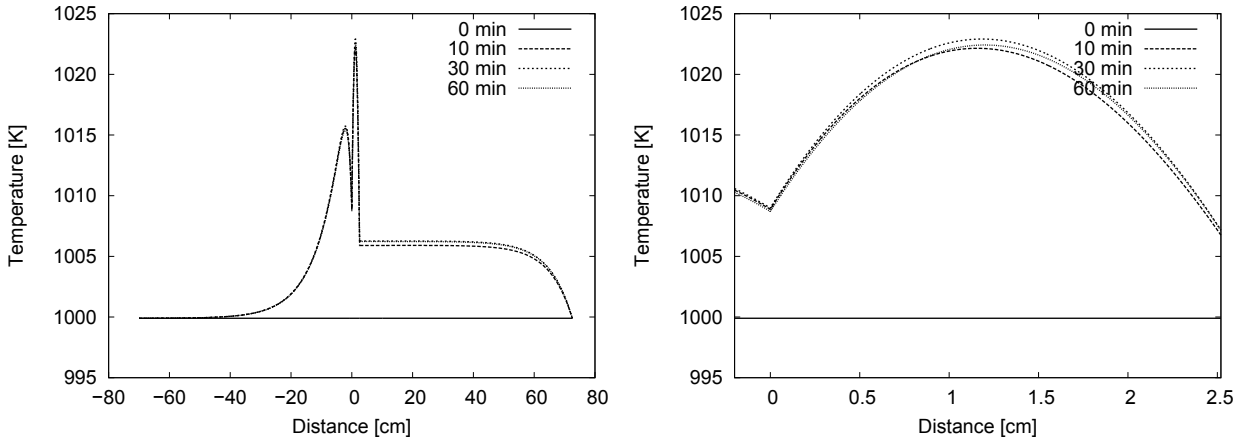

(a) Full domain (flow tube reactor). (b) FiberForm® sample.

Figure 10. Temperature as a function of time, with a variable fiber reactivity of $k_f = 10^5 e^{-1.2\times10^5/(RT)}$ m/s

by the model to be zero at all test conditions. As a consequence the value of $p2$ pressure at the end of the experiment is also poorly reproduced. Since the material does not recess, in order to match the experimental value of the mass loss, more material has to be lost inside. Consequently the permeability has to be higher, causing the numerical value of $p2$ to be higher at the end of the experiment. The discrepancy between the numerical and experimental values increases as T increases. Obtaining an accurate prediction of time and in-depth variations of the permeability appears to be of chief importance to accurately match the measured recession. Additionally, mechanical erosion phenomena, might have a significant role in the present experiments. As observed from the micrographs of the oxidized fiber, pitting caused by oxidation results in significant weakening of the fibers' structure. When stresses imposed by the flow exceed the strength of the oxidized material, carbon particles or dust will cause blockage effects and alter the actual permeability. In addition, the particles that are convected out of the sample (spallation) result in mass loss. The present model does not account for mass loss due to mechanical effects.

Table 3. Comparison between experiments (E) and numerical simulations (S)

Sample #	T, K	E/S	ΔT, K	$\Delta m/m_0$, %	$p_{2,0}$, Pa	$p_{2,end}$, Pa	$k_f \times 10^4$, m/s
a1	700	E	-	2.1	961	956	0.30
		S	2.1	2.0	962	1181	
a2	800	E	-	16.1	1119	1124	2.90
		S	11	15.9	1120	1748	
a3	900	E	-	19.4	1218	1246	4.25
		S	10	19.6	1212	1790	
a4	1000	E	7.5	23.3	1084	1125	5.90
		S	8.5	23.3	1087	1841	
a5	1100	E	11	21.6	81	417	-
		S	-	-	-	-	
a6	1200	E	13	28.7	577	787	9.00
		S	6.25	28.5	595	1866	
a7	1300	E	15	33.6	309	691	15.00
		S	6.25	34.0	350	1813	

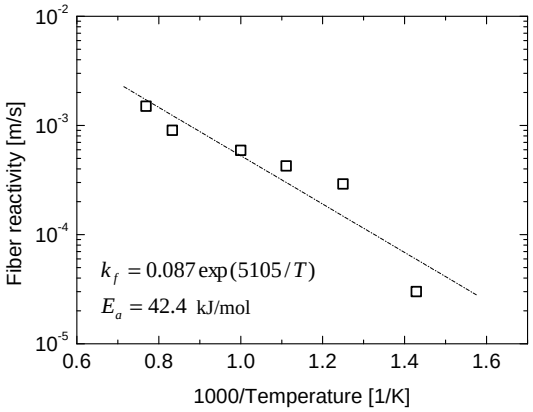

Figure 11. Fiber reactivity as a function of reciprocal temperature.

Values of the fiber reactivity obtained with the above approach are found to be between 10^{-5} and 10^{-3}. Reactivity data are plotted in Fig. 11 versus reciprocal temperature and fitted with an Arrhenius-type law of the form $k_f = A_f e^{-Ea/(RT)}$. From the fit, an activation energy of $E_a \approx 42.4$ kJ/mol is estimated.

Any comparison of reactivity data with values found in the literature is a particularly involved exercise because of several differences in the experimental setups used for the measurements and in the properties and characteristics of the materials investigated. The only known data on FiberForm® is documented in Ref. 7, where, at a temperature of 898 K, a value of $\approx 10^{-2}$ m/s was found, higher than the 4.25×10^{-4} m/s

measured in the present work at 900 K. The discrepancy can be attributed to: 1) the different inlet pressure for the experiment (12800 Pa vs. 1920 Pa), 2) the higher virgin FiberForm® density (184.5 kg/m^3 vs. 165 kg/m^3), and 3) the fact that the model used in Ref. 7 did not solve the momentum and energy equations, unlike the present work. Measurements obtained for carbon fibers manufactured from the same precursor,[18] using a different experimental arrangement, provided a fiber reactivity of 2.1×10^{-4} m/s at 898 K for a bulk density of 160 kg/m^3, similar to the present experiment. Probabilities of reaction γ of the order of 10^{-6} can be computed from the fiber reactivity as $\gamma = k_f \sqrt{(2\pi m)/(k_B T)}$, where m is the molecular mass and k_B is Boltzmann's constant. At temperatures below 900 K, these values are close to the reaction probabilities of graphite in molecular oxygen from Park[19] usually adopted in state-of-the-art models. Nevertheless, due to the lower activation energy found from the present experimental/numerical approach, values at higher temperatures are lower than Park's.

V. Conclusion

Material response experimental results obtained from a flow tube reactor facility were presented. Oxidation of FiberForm®, the carbon fiber preform of PICA, was investigated in air, at temperatures between 700 and 1300 K and a pressure of 2 kPa. A material response code based on a volume-averaged approach was used to evaluate the oxidation reactivity of carbon fibers, yielding results corresponding to data measured experimentally. Experiments were found to be dominated by reaction-controlled oxidation at the conditions analyzed. Fiber reactivities between $\approx 3 \times 10^{-5}$ and $\approx 1 \times 10^{-3}$, increasing with temperature, were computed. Overall, the code was able to accurately capture the physics of the phenomena observed, predicting with high fidelity the mass loss measured experimentally. Discrepancies in the values of surface recession suggested that further investigations should be carried out on the time-dependent in-depth oxidation of the material, aimed at characterizing the change in time of material properties like permeability and density.

VI. Acknowledgments

This work was supported by NASA SBIR Phase-2 Award NNX10CC53P and NASA EPSCoR Grant NNX13AN04A. Support by the Hypersonic EDL program for the effort is gratefully acknowledged. We thank F. S. Milos (NASA Ames Research Center) for the fruitful discussion on permeability. We are also thankful to S. A. Sepka and J. W. Ridge (ERC, Inc.) for the assistance at the flow-tube laboratory. The review comments of Y.-K. Chen and K. Skokova (NASA Ames Research Center) are greatly appreciated.

References

[1]Martin, A. and Boyd, I. D., "Modeling of heat transfer attenuation by ablative gases during Stardust re-entry," *50th AIAA Aerospace Sciences Meeting*, AIAA 2012-0814, Nashville, TN, January 9–12 2012.
doi:10.2514/6.2012-814

[2]Lachaud, J., Cozmuta, I., and Mansour, N. N., "Multiscale Approach to Ablation Modeling of Phenolic Impregnated Carbon Ablators," *Journal of Spacecraft and Rockets*, Vol. 47, No. 6, 2010, pp. 910–921.
doi:10.2514/1.42681

[3]Lachaud, J. and Mansour, N., "Porous-material Analysis Toolbox based on OpenFOAM-extend and Applications," *44th AIAA Thermophysics Conference*, AIAA Paper 2013-2767, American Institute of Aeronautics and Astronautics, June 2013.
doi:10.2514/6.2013-2767

[4]April, G. C., *Energy transfer in the char zone of a charring ablator*, Ph.D. thesis, Louisiana State University, Baton Rouge, LA, May 1st 1969.

[5]Panerai, F., Martin, A., Mansour, N., Sepka, S., and Lachaud, J., "Flow-tube Oxidation Experiments on the Carbon Preform of PICA," *44th AIAA Thermophysics Conference*, AIAA Paper 2013-2769, San Diego, CA, USA, 2013.
doi:10.2514/6.2013-2769

[6]McBride, B. J. and Gordon, S., "Computer Program for Calculation of Complex Chemical Equilibrium Compositions and Applications II. User's Manual and Program Description," Tech. Rep. NASA RP-1311-P2, NASA Lewis Research Center, 1996.

[7]Lachaud, J. R., Mansour, N. N., Ceballos, A., Pejaković, D., Zhang, L., and Marschall, J., "Validation of a volume-averaged fiber-scale model for the oxidation of a carbon-fiber preform," *42nd AIAA Thermophysics Conference*, AIAA 2011-3640, Honolulu, HI, 27-30 June 2011.
doi:10.2514/6.2011-3640

[8]Marschall, J. and Milos, F. S., "Gas Permeability of Rigid Fibrous Refractory Insulations," *Journal of Thermophysics and Heat Transfer*, Vol. 12, No. 4, October-December 1998, pp. 528–535.
doi:10.2514/2.6372

[9]Mansour, N. N., Panerai, F., Martin, A., Parkinson, D. Y., MacDowell, A., Haboub, A., Sandstrom, T. A., Fast, T., Vignoles, G. L., and Lachaud, J., "A New Approach To Light-Weight Ablators Analysis: From Micro-Tomography Measurements to Statical Analysis and Modeling," *44th AIAA Thermophysics Conference*, AIAA Paper 2013-2768, San Diego, CA, USA, 2013.
doi:10.2514/6.2013-2768

[10]Martin, A. and Boyd, I. D., "Non-Darcian behavior of pyrolysis gas in a thermal protection system," *Journal of Thermophysics and Heat Transfer*, Vol. 24, No. 1, Jan.-Mar. 2010, pp. 60–68.
doi:10.2514/1.44103

[11]Martin, A., "Modeling of chemical non equilibrium effects in a charring ablator," *51st AIAA Aerospace Sciences Meeting*, AIAA 2013-0301, Grapevine, TX, January 7–10 2013.
doi:10.2514/6.2013-301

[12]Sutton, K. and Gnoffo, P. A., "Multi-component diffusion with application to computational aerothermodynamics," *7th AIAA/ASME Joint Thermophysics and Heat Transfer Conference*, AIAA Paper 1998-2575, Albuquerque, NM, June 15-18 1998.
doi:10.2514/6.1998-2575

[13]Scoggins, J. B., *The Development of a Thermochemical Nonequilibrium Ablation and Pyrolysis Model for Carbon-Phenolic Thermal Protection Systems*, Master's thesis, North Carolina State University, 2011.

[14]Wilke, C., "A viscosity equation for gas mixtures," *J. Chem. Phys.*, Vol. 18, No. 4, 1950, pp. 517–519.
doi:10.1063/1.1747673

[15]Lachaud, J. and Mansour, N. N., "Microscopic scale simulation of the ablation of fibrous materials," *48th AIAA Aerospace Sciences Meeting and Exhibit*, AIAA Paper 2010-984, Orlando, FL, 4-7 January 2010.
doi:10.2514/6.2010-984

[16]Ellingham, H. J. T., "Reducibility of Oxides and Sulfides in Metallurgical Processes," *Journal of the Society of Chemical Industry*, Vol. 63, No. 5, 1944, pp. 125.
doi:10.1002/jctb.5000630501

[17]Martin, A., "Volume averaged modeling of the oxidation of porous carbon fiber material," *44th AIAA Thermophysics Conference*, AIAA Paper 2013-2636, San Diego, CA, Jun 24-28 2013.
doi:10.2514/6.2013-2636

[18]Lachaud, J., Bertrand, N., Vignoles, G., Bourget, G., Rebillat, F., and Weisbecker, P., "A theoretical/experimental approach to the intrinsic oxidation reactivities of C/C composites and of their components," *Carbon*, Vol. 45, 2007, pp. 2768.
doi:10.1016/j.carbon.2007.09.034

[19]Park, C., "Effects of Atomic Oxygen on Graphite Ablation," *AIAA Journal*, Vol. 14, No. 11, 1976, pp. 1640–1642.
doi:10.2514/3.7267